Journal of Solid State Electrochemistry
https://doi.org/10.1007/s10008-023-05500-2

ORIGINAL PAPER

Temperature effect on electrochemical properties of lithium manganese phosphate with carbon coating and decorating with MWCNT for lithium-ion battery

J. Herrera Robles[1] · H. Camacho Montes[2] · P. E. García Casillas[2] · C. Velasco-Santos[3] · A. L. Martínez-Hernández[3] · O. Raymond Herrera[4] · J. A. Matutes Aquino[5] · L. Fuentes Coba[5] · L. Alvarez Contreras[5] · R. K. Bordia[1]

Received: 3 August 2022 / Revised: 22 March 2023 / Accepted: 31 March 2023

Abstract
The increasing demands for higher energy density and higher power capacity of Li-ion secondary batteries have led to a search for electrode materials whose capacities and performance are better than those available today. One promising candidate is lithium manganese phosphate, and it is necessary to understand its transport properties. These properties are crucial for designing high-power Li-ion batteries. The effect on the electronic conductivity is analyzed with a conductor material, carbon nanotubes multi-walled, and glucose was used as a carbon source. Here, the transport properties of $LiMnPO_4$, $LiMnPO_4$/C, and $LiMnPO_4$/MWCNT are investigated using impedance spectroscopy. The electronic conductivity is found to increase with increasing the temperature from 2.92×10^{-5} S cm^{-1} to 6.11×10^{-5} S cm^{-1}. The magnetization properties are investigated, and antiferromagnetic behavior below 34 K is reported for the three compositions. The structural characterizations were studied to confirm the phase formation of material with XRD, TEM, and SEM.

Keywords Olivine structure · MWCNT · Magnetic behavior · Electrochemical properties

Introduction

Zero emissions and renewable energy technologies have become important options to mitigate greenhouse gas emissions and form an independent carbon cycle to reduce global warming. Solar, wind, and tidal powers have been used as alternative energy sources. These power systems are generally used in the electrical supply grid for the generation and supply of auxiliary power. The support mechanism has enhanced the efficiency and quality of the production and storage of renewable energy sources [1]. Olivine-structured lithium transition-metal phosphate has attracted broad attention as a potential Li-ion battery cathode material to replace transition metal oxide-based materials such as $LiCoO_2$ [2, 3]. Lithium-ion batteries have been intensively investigated in recent years. The reason is that there has been increasing demand in the portable electronics market and its application in electric vehicles (EVs) and hybrid electric vehicles (EHVs). The phospho-olivine $LiMPO_4$ (M = Fe, Mn, Co, Ni) has been investigated and used in cylindrical batteries since the pioneering work of Goodenough et al. as a candidate positive electrode material for use in lithium rechargeable batteries [4–7]. This family of phosphate compounds has a three-dimensional framework stabilized by strong covalent bonds between oxygen ions and P^{5+}, resulting in PO_4^{3-} tetrahedral polyanions. These compounds are promising as a cathode material due to their high safety, environmental tolerability, and low cost. Olivine structured lithium manganese

✉ J. Herrera Robles
joel.herrera@uacj.mx

1 Department of Materials Science & Engineering, Clemson University, 161 Sirrine Hall, Clemson, SC 29634 0971, USA

2 Instituto de Ingeniería y Tecnología, Universidad Autónoma de Ciudad Juárez, Av. Del Charro 450 Norte Cd. Juárez, Chihuahua 32310, México

3 División de Estudios de Posgrado E Investigación, Instituto Tecnológico de Querétaro, Av. Tecnológico S/N, Colonia Centro Histórico, Santiago de Querétaro, Querétaro 76000, México

4 Centro de Nanociencias y Nanotecnología, Universidad Nacional Autónoma de México, Km. 107 Carretera Tijuana-Ensenada, AP. 14, Ensenada, Baja California 22860, México

5 Centro de Investigación en Materiales Avanzados, Miguel de Cervantes 120, Chihuahua 31109, Chihuahua, México

Published online: 13 April 2023

phosphate ($LiMnPO_4$) as a cathode material for lithium-ion batteries is having a high capacity (170 mAh g^{-1}) and high redox potential (4.1 V vs Li^+), respectively. Moreover, $LiMnPO_4$ has a 20% greater energy density compared to $LiFePO_4$ [8], working ability at high temperatures, low cost, and is eco-friendly which makes $LiMnPO_4$ a successful cathode candidate for lithium-ion batteries [9]. In spite of these properties, poor electrical conductivity is a crucial issue to be addressed [10]; to overcome it, one of the good ways is through surface coating with a carbon source [11, 12]. Luo et al. obtained $LiMnPO_4$/C via citric acid-assisted sol–gel method [13]. Their work demonstrated that $LiMnPO_4$/C obtained at 500 °C for 10 h has good structural ability and electrical properties. Kwon et al. adopted the sol–gel method to prepare $LiMnPO_4$/C using anhydrous ethanol as solvent, and graphene nanoplates (GNP) were added into terminal material by ball milling [14]. Zhong et al. performed different compositions of $LiMnPO_4$ electrodes with addition of multi-walled carbon nanotubes (MWCNTs) [15]; Zong and Liu reported hydrothermal approach and solid-state reaction to synthesis of LMP compound and carbon-coated LMP samples with carbon nanotubes [16]. Thermal stability is a characteristic of the degradation of the battery due to high temperatures generated during charge–discharge cycles; the cathode after several cycles tends to decompose and release oxygen which promotes runaway reactions with the electrolyte. But there is still lacking information on solid-state analysis which is an alternative to improving the electrochemical properties of this material. The majority of studies of $LiMnPO_4$ have focused on electrolyte systems; in this work, we think that it is a good approach to analyze the previous functionalization of electrolyte systems. In the present study, the analysis and comparison of the crystal structure, morphology, impedance values, and electrochemical properties of the conductive $LiMnPO_4$ $LiMnPO_4$/C and $LiMnPO_4$/MWCNT composites are addressed.

Experimental procedure

The sol–gel method was used to synthesize the powders. As starting precursors, manganese (II) acetate tetrahydrate ($C_6H_6MnO_6 \times 4H_2O$, 99.9% Aldrich 229,776), ammonium phosphate dibasic ($(NH_4)_2HPO_4$, 98% Aldrich 7783–28-0), and lithium acetate dihydrate ($CH_3COOLi \times 2H_2O$, Aldrich, 6108–17-4) are separately dissolved in deionized water at 60 °C in beakers 1:1:1:1 molar ratio under constant stirring. Afterward, all solutions are mixed under constant stirring for 1 h and then dried at 150 °C for 24 h in the oven. The obtained xerogel is grinded in a mortar and pestle, and then fired under reducing atmosphere with 90% argon and 10% hydrogen at 500 °C for 6 h. For the carbon coating, the same procedure is followed; the only difference is the moment when all the solutions are mixed, the glucose is added as a carbon source in a 1:2 molar ratio. To decorate with MWCNT, carbon nanotubes and powders $LiMnPO_4$ are mixed in a 1:2 molar ratio under stirring. Then, 0.75 ml of H_2SO_4 and 10 ml of distilled water, 50 mg of malic acid, and $KMnO_4$ are added and put under constant stirring at 60 °C, then it is washed several times with distilled water to reach pH = 7. It dried at room temperature for 24 h.

The sample was characterized using X-ray diffraction analysis (XRD) in a *Panalytical X'pert Pro* with X-rays source of Cu K-alpha. The structural characterization was performed by scanning electron microscopy, using SEM JSM 5800-LV and transmission electron microscopy, using TEM JEM-2200FS. Magnetic behavior is analyzed through room temperature vibrating sample magnetometer studies. The structural magnetic behavior was studied using an LDJ VSM9600 Cryogen-free Physical Property Measurement System, and curves were measured from 5 to 300 K. Compacted pellets were prepared from the powder by pressing at 340 MPa for 60 s, forming cylindrical samples of 14 mm in diameter; the pellets were put under heat treatment under controlled atmosphere (90% argon and 10% hydrogen) at 500 °C for 6 h. For electrochemical properties, the pellets were polished on both sides and painted with silver paste on both surfaces forming the cell configuration Ag ‖ LiMPO ‖ Ag. The pellets were subsequently heated at 80 °C for 5 h in order to remove the organic solvent. Electrochemical impedance spectroscopy was employed to measure the electrical conductivity using CS series electrochemical Workstation in the frequency range 0.01 Hz–100 kHz. The measurements were performed at temperatures 45, 50, 55, and 60 °C. The sample temperature was measured by a thermocouple placed near the sample. The ionic diffusivity was measured by electrochemical impedance spectroscopy. EIS was measured over a range of frequency 0.01 Hz–100 kHz at AC amplitude of 10 mV with the same range of temperatures as in the electrical measured. The measure was performed in a Swagelok-type cell, polyethylene oxide was used as an electron blocking, lithium conducting layer.

Results and discussion

XRD

Figure 1 shows the XRD patterns for pure $LiMnPO_4$, $LiMnPO_4$/MWCNT, and $LiMnPO_4$/C composites. The three patterns can be indexed to an orthorhombic olivine-type structure with space group *Pnmb*, and there is no secondary phase in each pattern. For $LiMnPO_4$/C samples, the carbon phase is amorphous, and then it only affects the X-ray pattern background. As the added carbon amount is small, it only has a small influence on the background. The peaks for MWCNT are localized for 2θ less than 10° with very low

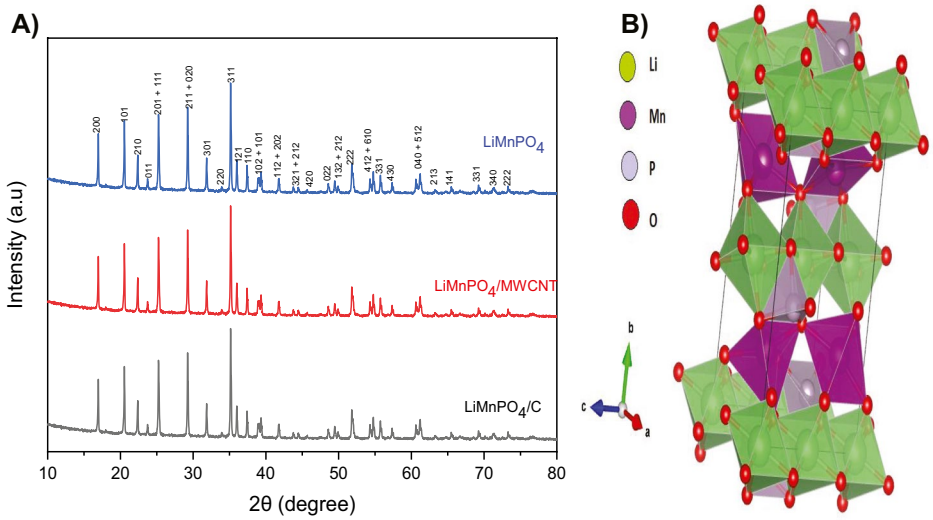

Fig. 1 X-ray diffraction patterns of $LiMnPO_4$, $LiMnPO_4$/C, and $LiMnPO_4$/MWNT. All peaks correspond to the crystallographic phase according to 167251-ICSD record and the crystal structure of $LiMnPO_4$. Light green polyhedrons represent LiO_6 octahedra, purple represents MO_6 octahedra, and light purple polyhedrons represent PO_4 tetrahedra

intensity [17], and the present XRD patterns were run for values higher than that. In order to find out if each carbon source affected the crystal structure, the crystallite size (D) was calculated by Scherrer formula $D = 0.9\,\lambda/\beta\cos\Theta$, where λ is the X-ray wavelength, β is the width and half maximum (FWHM), and Θ is the Bragg angle. To estimate the FWHM values, the four highest peaks corresponding to (101), (201), (211), and (311) directions were used. The calculated values are 55, 58, and 46 nm for pristine and composites with glucose and MWCNT, respectively. It is believed that the small particle size is useful for the intercalation/de-intercalation process of lithium ions [18]; in this work, we used glucose and MWCNT carbon source to increase electronic conductivity and promoted better diffusion which was demonstrated in the electrochemistry properties further. Table 1 summarizes some lattice parameters in which those of the pristine phase coincide with previous reports [19].

SEM

The morphological structure of the samples was analyzed by SEM and TEM micrographs which are shown in Fig. 2. The pristine sample (Fig. 2a, b) is composed of a few agglomerates up to several microns and many submicron grains. Carbon coating can be seen in Fig. 2c and here clearly shows the difference in several microns in the agglomerates where the particles are interconnected by the carbon resulting from glucose. Figure 2e depicts the TEM image where the carbon layer on the surface of the sample can be clearly identified. In Fig. 2f–h, TEM images for $LiMnPO_4$/MWCNT sample are shown. The use of sulfuric acid leads to chemistry oxidation and permits carboxylic groups to be formed; through this way, the $LiMnPO_4$ and carbon nanotubes could be connected through an ester bond, and this process has demonstrated to create moieties to bond new reactive chains that improve compatibility with other materials and allow taking advantage of MWCNT properties [20, 21]. This kind of treatment may create defects in the sidewalls of the MWCNT also decreasing the oxidized surface which allows adherence of the powders and MWCNT. The addition of $KMnO_4$ and malic acid was to achieve better dispersion of MWCNT on the surface of $LiMnPO_4$ [22]. Furthermore, porosity and interconnected networks of carbon nanotube are clearly noted. This framework enhances ion diffusion during the insertions and extraction process.

Table 1 Lattice parameters of $LiMnPO_4$, $LiMnPO_4$/C, and $LiMnPO_4$/MWCNT

Sample	a (Å)	b (Å)	c (Å)	V (Å^3)
$LiMnPO_4$	6.106	10.445	4.744	302.558
$LiMnPO_4$/C	6.125	10.451	4.751	303.247
$LiMnPO_4$/MWCNT	6.121	10.441	4.745	304.122

Magnetic structure behavior

The magnetization curves are linear over the investigated temperature and magnetic field ranges. The deviations from such behavior are indicative of structural defects and/or impurities [23]. The $LiMnPO_4$ compound is a Curie–Weiss paramagnet at room temperature and undergoes antiferromagnetic transitions with collinear magnetic structures, but different spin orientations [24]. The magnetic transition metal ions occupy the distorted octahedral M2 site forming corner-sharing MO_6 units which are separated by the PO_4 tetrahedra and edge-sharing LiO_6 octahedra. The magnetization of $LiMnPO_4$,

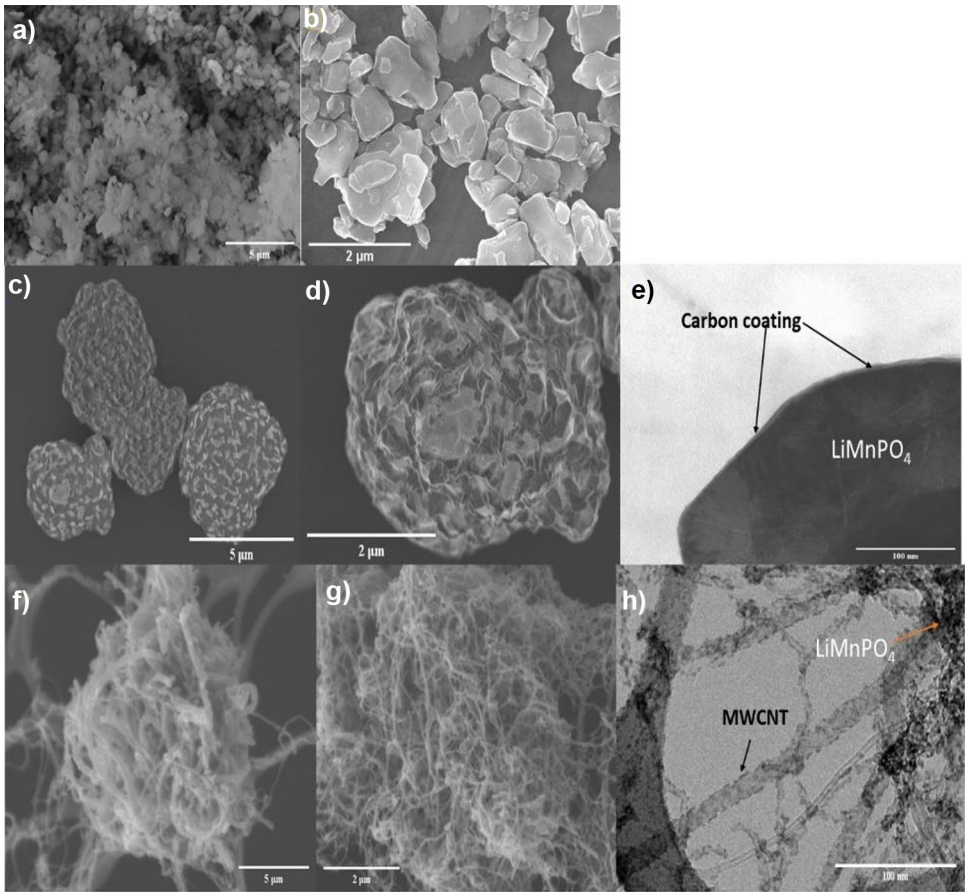

Fig. 2 SEM and TEM images. Pristine sample $LiMnPO_4$ (**a**, **b**). Carbon-coated $LiMnPO_4$/C (**c**, **d**, **e**) TEM image. $LiMnPO_4$/MWCNT (**f**, **g**, **h**) TEM image

$LiMnPO_4$/C, and $LiMnPO_4$/MWCNT is shown in Fig. 3 recorded over a range of fields, and the magnetization increases linearly with the applied field. The alignment of the spins to the applied field promotes the paramagnetic behavior, and the magnetic susceptibility is positive. The lack of ferromagnetic behavior indicates the absence of different valance states which suggest negligible contribution from the electronic part, and it indicates the nature of the ion conductivity of these materials. The temperature dependence of the inverse magnetic susceptibility was analyzed. All compounds exhibit a Curie–Weiss type dependence temperature for an antiferromagnetic ground state below the Nee temperature that is reported $T_N = 34$ K (Fig. 4). Values

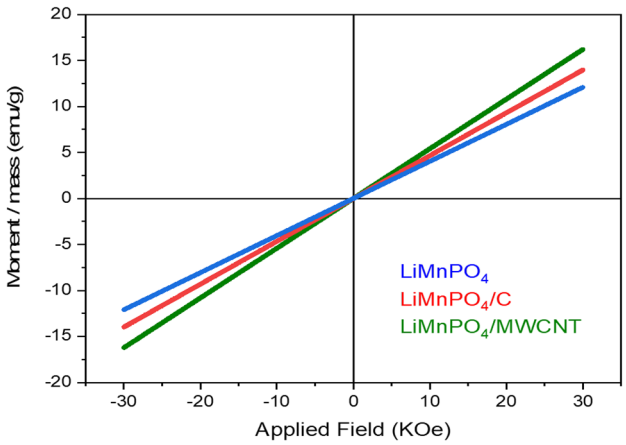

Fig. 3 Magnetization versus applied magnetics field at room temperature for $LiMnPO_4$, $LiMnPO_4$/C, and $LiMnPO_4$/MWCNT

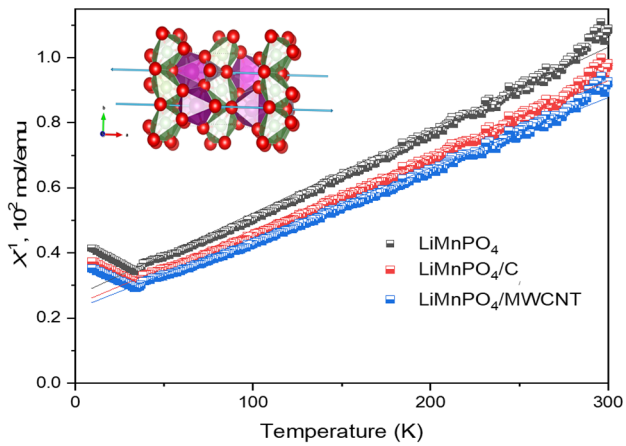

Fig. 4 The temperature depends on the magnetic susceptibility of $LiMnPO_4$, $LiMnPO_4$/C, and $LiMnPO_4$/MWCNT

for effective magnetic moment μ_{eff} are calculated by $X^{-1} = (T - \Theta)/C_m$ and $\mu_{eff} = \sqrt{8C_m\mu_B}$, where Θ is the Weiss temperature, C_m is the Curie constant, and μ_B is the Bohr magneton. The effective magnetic moment of Mn^{2+} in pure $LiMnPO_4$ is consistent with a spin-only value of 5.91 BM; this suggests that the manganese ions are in 2 + states. The value for the Curie constant corresponds to 4.61 emu K/mol. For the samples coated with carbon, the results have a slight variation of ≤ 0.02. These results are consistent with previous reports [25]. Clearer evidence of defects is antisite defect; when Mn and Li switch sites, magnetic properties should be sensitive to these structural modifications; for example, dilution of the transition metal sublattice with non-magnetic ions may lead to a decrease of T_N and absolute Θ values [26]. This analysis lets us know that our samples are out of impurities that many times cannot be detected by classical characterization.

Electrochemical properties

The electrochemical impedance spectra were analyzed in the frequency range 0.01 Hz–100 kHz, and the Nyquist plot is shown in Fig. 5 of pristine, carbon-coated, and multi-walled carbon nanotube decorated samples. The impedance spectra were measured at 45 °C, 50 °C, 55 °C, and 60 °C temperatures with the configuration Ag ‖ LiMPO ‖ Ag. The absence of an additional polarization process at low frequencies (i.e., a second semicircle) indicates that the electronic carries conduction predominately, and it also suggests negligible ionic conductivity. All the samples were evaluated with the ideal equivalent circuit; the semicircle is assigned in this work as R1 which represents the interfacial charge transfer resistance, and CPE (constant phase element) stands as the typical electrical double-layer capacitance (Fig. 5d). As shown in Table 2, the composition $LiMnPO_4$/MWCNT exhibits the highest electronic conductivity. Previous works

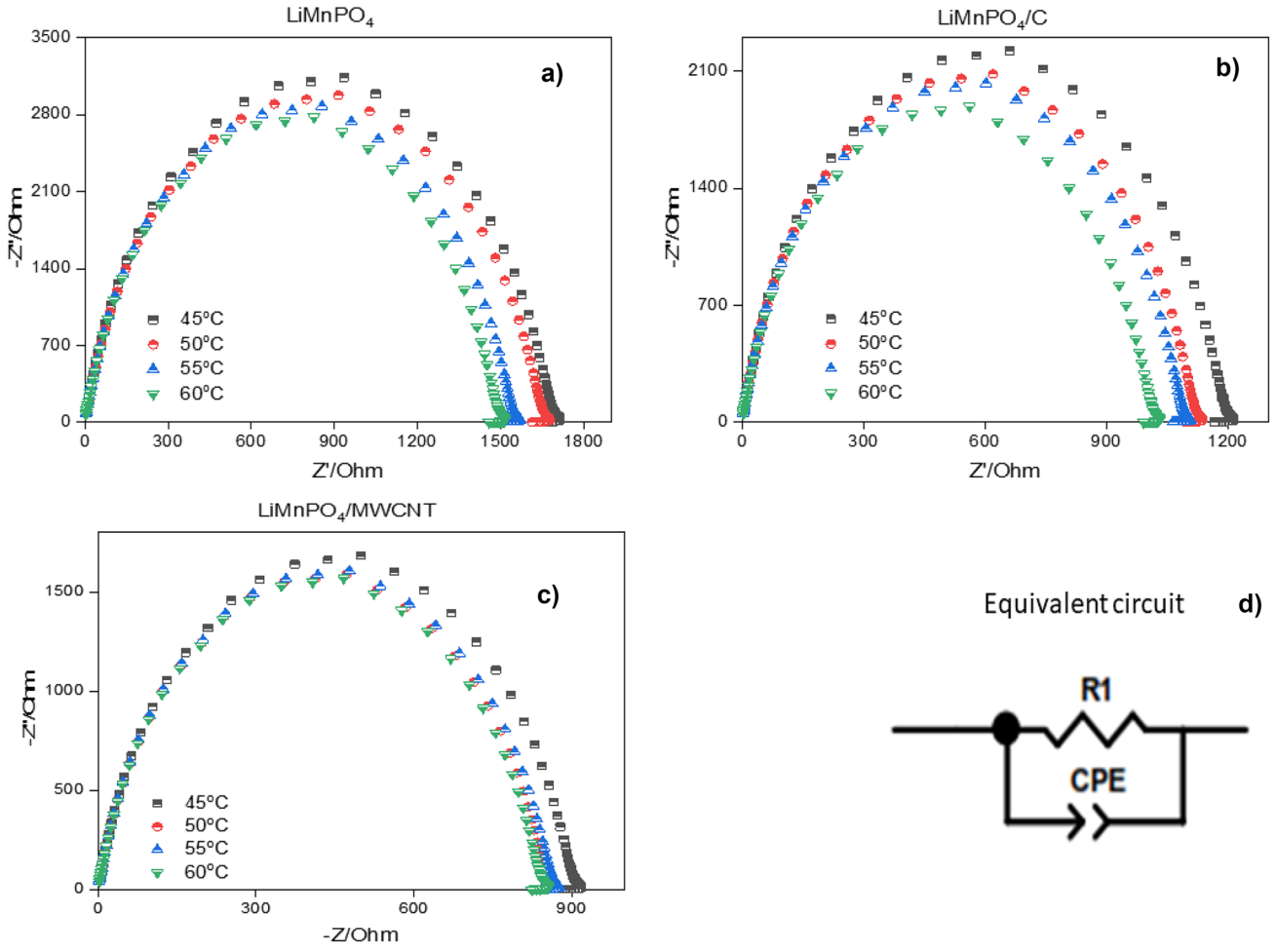

Fig. 5 **a**, **b**, **c** Electrochemical impedance spectral characterization of the samples $LiMnPO_4$, $LiMnPO_4$/C, and $LiMnPO_4$/MWCNT, and **d** equivalent circuit to evaluate the impedance spectra

Table 2 Charge transfer resistance, electronic conductivity, and diffusivity were measured at different temperatures

T °C	R_{ct} (Ω)	Diffusivity $cm^2\ s^{-1}$	Conductivity $S\ cm^{-1}$	Composition
45	1.73×10^{4}	1.48×10^{-14}	$2.92\times10^{-1\circ}$	
50	1.66×10^{4}	1.55×10^{-14}	$3.06\times10^{-1\circ}$	**$LiMnPO_4$**
55	1.58×10^{4}	1.82×10^{-14}	$3.21\times10^{-1\circ}$	
60	1.52×10^{4}	2.04×10^{-14}	$3.34\times10^{-1\circ}$	
45	1.21×10^{3}	2.08×10^{-13}	4.18×10^{-9}	
50	1.14×10^{3}	2.29×10^{-13}	4.44×10^{-9}	**$LiMnPO_4$/C**
55	1.08×10^{3}	2.51×10^{-13}	4.69×10^{-9}	
60	1.02×10^{3}	2.84×10^{-13}	4.97×10^{-9}	
45	19,136.11	2.57×10^{-13}	5.22×10^{-9}	
50	17,764.54	2.88×10^{-13}	5.62×10^{-9}	**$LiMnPO_4$/MWCNT**
55	17,064.68	3.41×10^{-13}	5.86×10^{-9}	
60	16,374.29	4.55×10^{-13}	6.11×10^{-9}	

reported the electrochemical reactions on different heat treatment temperatures of $LiMnPO_4$ materials synthesized by several approaches determined by EIS [27–29]. The pure $LiMnPO_4$ phase presents very low electronic intrinsic properties as well as low ionic conductivity, manifesting this in poor electrochemical properties [30]. This poor response is attributed to the low diffusion of lithium atoms between particles. A carbon source provides the conductive path for the diffusion of the ions [31]; among the several options as a carbon source, the MWCNT is getting attention due to its high symmetry which provides an excellent path for ionic and electronic conductivity. The conductivities for the three compositions measured at a given temperature increase with respect to the sample sequence: $LiMnPO_4$, $LiMnPO_4$/C, and $LiMnPO_4$/MWCNT. The result of the pristine sample is in good agreement with a previous report [32]. For the samples with carbon source and MWCNT, we found a remarkable increase in the conductivities. The values of activation energy, calculated using Arrhenius law, are displayed in Fig. 6; these results suggest a polaron conduction mechanism that is supported by temperature dependence [33]. It is well known that carbon coating is a good approach to improving electronic conductivity. The lowest value of 0.03 eV of activation energy is reported for decorated MWCNT, and this facilitates the conductivity.

The analysis with electron blocking cells takes into account the temperature-dependence of ionic diffusivity. Figure 7 shows the impedance spectra of $LiMnPO_4$ (Fig. 7a), $LiMnPO_4$/C (Fig. 7b), and $LiMnPO_4$/MWCNT (Fig. 7c) measured at 45 °C, 50 °C, 55 °C, and 60 °C. In contrast to the ion-blocking cells above reported, these impedance spectra consist of one semicircle at high frequencies, followed by a Warburg response at low frequencies. The high-frequency semicircle represents the total resistance to the charge (R1), which means electronic and ionic motion. The Warburg response is indicative of the diffusion of ions polarization owing to block electrons (W), and CPE represents the constant phase of the electrical double-layer capacitance; the impedance spectra were fitted with the equivalent circuit as shown in Fig. 7d. The lithium diffusion coefficient D can be calculated using the following equation [34]:

$$D = \frac{R^2T^2}{2A^2n^4F^4C^2\sigma^2} \tag{1}$$

where T is the room absolute temperature, R is the gas constant, A is the surface area of the electrode, F is the Faraday constant, n is the number of electrons per molecule attending the electronic transfer reaction, and C is the concentration of lithium ion in the $LiMnPO_4$ electrode. The plots of Z_{re} against $\omega^{1/2}$ are in Fig. 8, according to Eq. (2), and σ is the slope of the straight line:

$$Z'' = \sigma\omega^{-1/2} \tag{2}$$

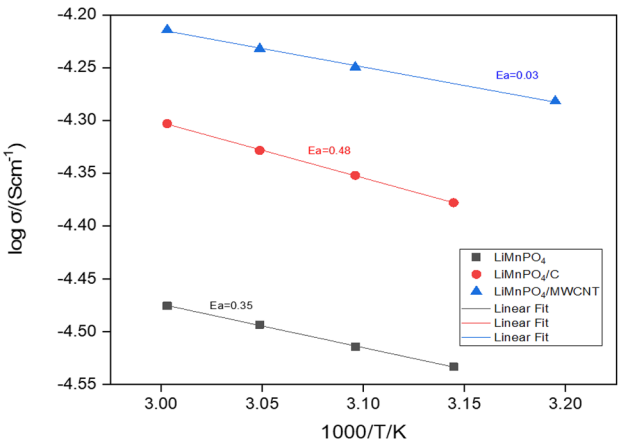

Fig. 6 Calculated activation energy using the Arrhenius equation as a function of the inverse temperature of $LiMnPO_4$, $LiMnPO_4$/C, and $LiMnPO_4$/MWCNT samples

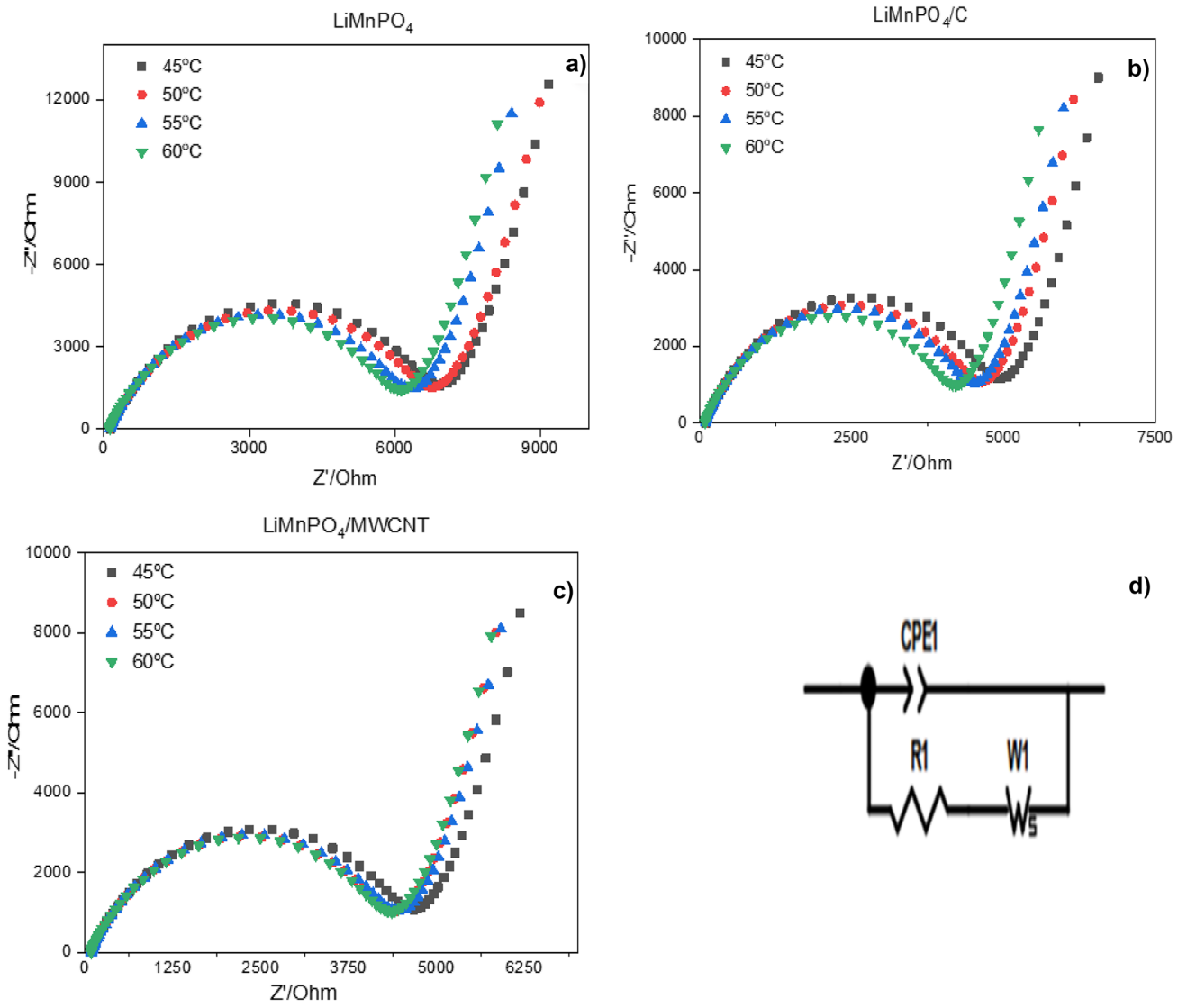

Fig. 7 **a**, **b**, **c** Electrochemical impedance spectral characterization of the samples $LiMnPO_4$, $LiMnPO_4$/C, and $LiMnPO_4$/MWCNT with electron blocking cell configuration; **d** equivalent circuit to evaluate the impedance spectra

The lithium diffusion coefficient D ($cm^2\ s^{-1}$) calculated with Eq. (1) is shown in Table 2, using the above-obtained σ with the plots in Fig. 8. Previous works reported the diffusion coefficient of $LiMnPO_4$ materials. Xiao et al. [35] and Han et al. [36] reported lithium diffusion coefficients of 5×10^{-14} $cm^2\ s^{-1}$ and 8×10^{-14} $cm^2\ s^{-1}$, respectively, for solvothermal prepared $LiMnPO_4$ materials. Pan et al. [37] D_{Li+} of 2×10^{-14} $cm^2\ s^{-1}$ obtained in solid-state approach. Wang et al. [38] investigated the effect of the high-energy ball milling time on the lithium diffusion properties in $LiMnPO_4$ synthesized by a soft template method. They showed that milling time affects the electrochemically evaluated lithium diffusion coefficient, reporting D_{Li+} within 10^{-16}–10^{-13} $cm^2\ s^{-1}$ range.

The results herein reported agree with current literature works suggesting the hindered kinetics of lithium insertion/deinsertion for $LiMnPO_4$. This severe issue represents the main problem limiting the effective employment of Mn-based olivines as cathodes in lithium batteries [39, 40].

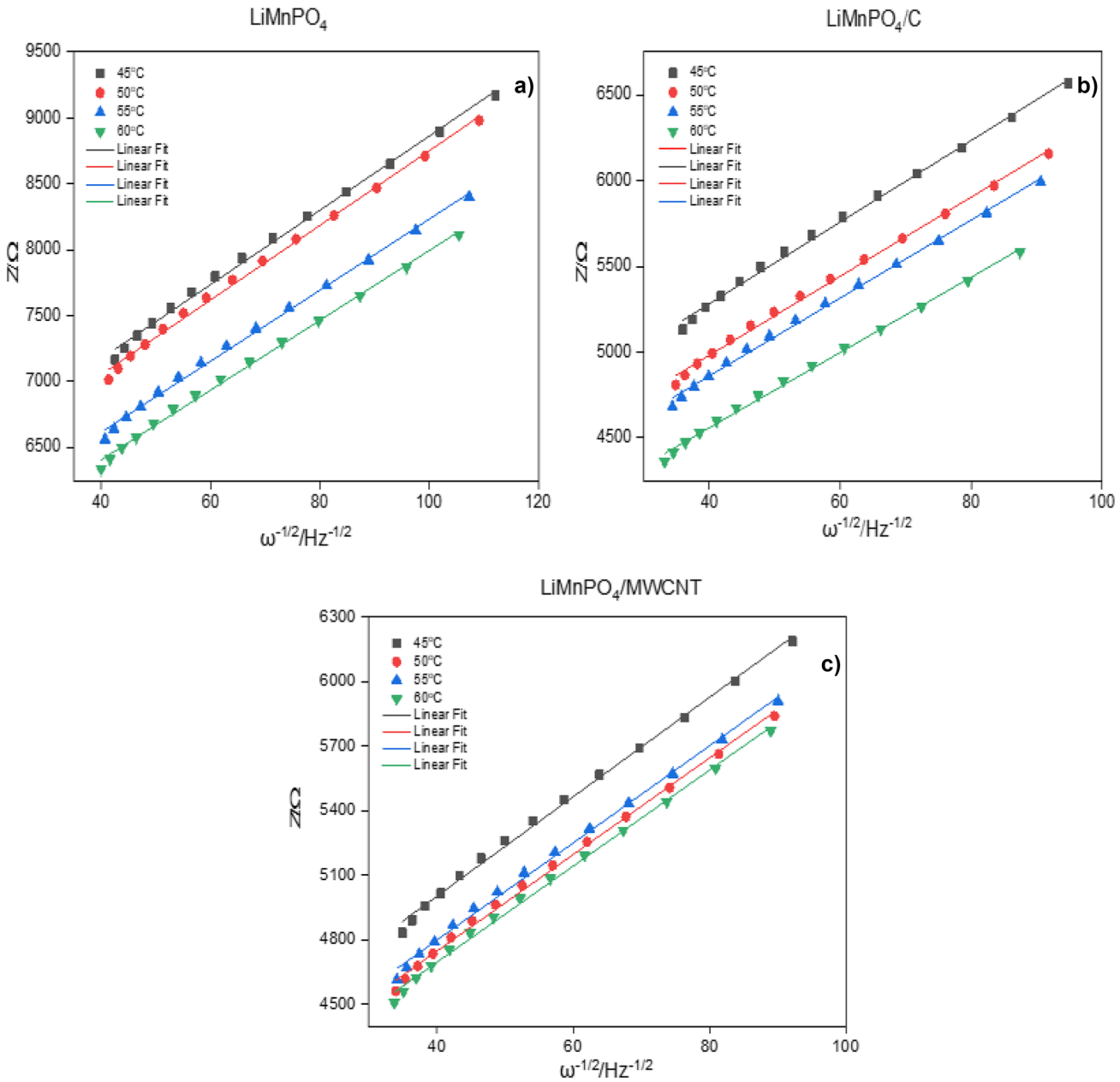

Fig. 8 Plots of the real component Z' vs $\omega^{-1/2}$ in the Warburg region for the impedance spectra of Fig. 7 and related linear fit

Conclusions

Electronic and lithium ionic transport in $LiMnPO_4$, $LiMnPO_4$/C, and $LiMnPO_4$/MWCNT have been measured using ion and electron blocking cell configurations. SEM and TEM revealed the well and uniformly decorated with MWCNT. The $LiMnPO_4$ pristine presented a higher charge transfer resistance, and the electronic conductivity and diffusivity of $LiMnPO_4$/MWCNT composite in the function of the temperature applied are higher than that of pure $LiMnPO_4$ and $LiMnPO_4$/C. The added MWCNTs not only increase the electronic conductivity and the lithium-ion diffusion coefficient but also decrease crystallite size and the charge transfer resistance. A comparison of these values with literature reports suggested that the lithium diffusion and conductivity evaluation is strongly affected by the structural and morphological characteristics and the adopted experimental setup used for evaluation. This evaluation could give a good sight previous to the use the electrolyte in future works.

Supplementary Information The online version contains supplementary material available at https://doi.org/10.1007/s10008-023-05500-2.

References

1. Yang Z, Zhang J, Kintner-Meyer MCW, Lu X, Choi D, Lemmon JP, Liu J (2011) Electrochemical energy storage for green grid. Chem Rev 111(5):3577–3613. https://doi.org/10.1021/cr100290v
2. Kim JK, Shin CR, Ahn JH, Matic A, Jacobsson P (2011) Highly porous $LiMnPO_4$ in combination with an ionic liquid-based polymer gel electrolyte for lithium batteries. Electrochem Commun 13(10):1105–1108. https://doi.org/10.1016/j.elecom.2011.07.005
3. Wani TA, Suresh G (2021) A comprehensive review of $LiMnPO_4$ based cathode materials for lithium-ion batteries: current strategies to improve its performance. J Energy Storage 44:103307. https://doi.org/10.1016/j.est.2021.103307
4. Chung SY, Bloking JT, Chiang YM (2002) Electronically conductive phospho-olivines as lithium storage electrodes. Nat Mater 1(2):123–128. https://doi.org/10.1038/nmat732
5. Martha SK, Markovsky B, Grinblat J, Gofer Y, Haik O, Zinigrad E, Aurbach D, Drezen T, Wang D, Deghenghi G, Exnar I (2009) $LiMnPO_4$ as an advanced cathode material for rechargeable lithium batteries. J Electrochem Soc 156(7):A541. https://doi.org/10.1149/1.3125765
6. Yang L, Luo S, Wang Y, Zhan Y, Wang Q, Zhang Y, Liu X, Mu W, Teng F (2020) Excess capacity on compound phases of Li2FeTiO4 composite cathode materials synthesized by hydrothermal reaction using optional titanium sources to boost battery performance. Chin Chem Lett 31(12):3200–3204. https://doi.org/10.1016/j.cclet.2020.05.036
7. Li S, Luo S, Yang L, Wang Q, Zhang Y, Liu X (2021) Synthesis and electrochemical properties of LiFePO4 cathode material by ionic thermal method using eutectic mixture of tetramethyl ammonium chloride–urea. Rare Met 40(12):3477–3484. https://doi.org/10.1007/s12598-021-01783-4
8. Padhi AK, Nanjundaswamy KS, Goodenough JB (1997) Phospho-olivines as positive-electrode materials for rechargeable lithium batteries. J Electrochem Soc 144(4):1188–1194. https://doi.org/10.1149/1.1837571
9. Drezen T, Kwon NH, Bowen P, Teerlinck I, Isono M, Exnar I (2007) Effect of particle size on $LiMnPO_4$ cathodes. J Power Sources 174(2):949–953. https://doi.org/10.1016/j.jpowsour.2007.06.203
10. Su J, Liu ZZ, Long YF, Yao H, Lv XY, Wen YX (2015) Enhanced electrochemical performance of $LiMnPO_4$/C prepared by microwave-assisted solvothermal method. Electrochim Acta 173:559–565. https://doi.org/10.1016/j.electacta.2015.05.105
11. Herrera Robles JO, Fuentes Cobas LE, Díaz De La Torre S, Camacho Montes H, Elizalde Galindo J, García Casillas PE, Rodríguez González CA, Álvarez Contreras L (2015) Synthesis and structural characterization of manganese olivine lithium phosphate. J Alloy Compd 643:S236–S240. https://doi.org/10.1016/j.jallcom.2014.11.114
12. El Khalfaouy R, Addaou A, Laajeb A, Lahsini A (2019) Synthesis and characterization of Na-substituted $LiMnPO_4$ as a cathode material for improved lithium-ion batteries. J Alloy Compd 775:836–844. https://doi.org/10.1016/j.jallcom.2018.10.161
13. Luo SH, Sun Y, Bao S, Li J, Zhang J, Yi TF (2019) Synthesis of Er-doped $LiMnPO_4$/C by a sol-assisted hydrothermal process with superior rate capability. J Electroanal Chem 832:196–203. https://doi.org/10.1016/j.jelechem.2018.10.062
14. Kwon N, Mouck-Makanda D, Fromm K (2018) A review: carbon additives in $LiMnPO_4$- and $LiCoO_2$-based cathode composites for lithium ion batteries. Batteries 4(4):50. https://doi.org/10.3390/batteries4040050
15. Zhong SK, Wang Y, Liu JQ, Wang J (2012) Synthesis of $LiMnPO_4$/C composite material for lithium-ion batteries by sol-gel method. Trans Nonferrous Metals Soc China 22(10):2535–2540. https://doi.org/10.1016/s1003-6326(11)61497-0
16. Zong J, Liu X (2014) Graphene nanoplates structured $LiMnPO_4$/C composite for lithium-ion battery. Electrochim Acta 116:9–18. https://doi.org/10.1016/j.electacta.2013.10.176
17. Chiu TM, Barraza-Fierro J, Castaneda H (2017) Comprehensive interfacial mechanisms of $LiMnPO_4$-MWCNT composite ratios in acidic aqueous electrolyte. Electrochim Acta 253:93–103. https://doi.org/10.1016/j.electacta.2017.09.018
18. Sharmila V, Parthibavarman M (2021) Lithium manganese phosphate associated with MWCNT: enhanced positive electrode for lithium hybrid batteries. J Alloys Compd 858:157715. https://doi.org/10.1016/j.jallcom.2020.157715
19. Pierson HO (2012) Handbook of carbon, graphite, diamonds, and fullerenes: properties, processing, and applications. William Andrew
20. Jin B, Jin EM, Park KH, Gu HB (2008) Electrochemical properties of $LiFePO_4$-multiwalled carbon nanotubes composite cathode materials for lithium polymer battery. Electrochem Commun 10(10):1537–1540. https://doi.org/10.1016/j.elecom.2008.08.001
21. Kirsanova MA, Ryazantsev SV, Abakumov AM (2020) Anionic substitution in $LiMnPO_4$: the $Li_{1-x}Mn_{1+x}(PO4)_{1-y-z}(VO4)_y(OH)_{4z}$ solid solutions prepared with a microwave-assisted hydrothermal method. J Solid State Chem 286:121294. https://doi.org/10.1016/j.jssc.2020.121294
22. Velasco-Santos C, Velasco-Santos C, Castaño VM (2010) Carbon nanotubes composites: processing, grafting and mechanical and thermal properties. Curr Nanosci 6(1):12–39. https://doi.org/10.2174/157341310790226270
23. Kwon NH, Drezen T, Exnar I, Teerlinck I, Isono M, Graetzel M (2006) Enhanced electrochemical performance of mesoparticulate $LiMnPO_4$ for lithium ion batteries. Electrochem Solid-State Lett 9(6):A277. https://doi.org/10.1149/1.2191432
24. Zhang S, Lu F, Zheng L (2011) Dispersion of multiwalled carbon nanotubes (MWCNTs) by ionic liquid-based Gemini pyrrolidinium surfactants in aqueous solution. Colloid Polym Sci 289(17–18):1815–1819. https://doi.org/10.1007/s00396-011-2500-2
25. Chen J, Vacchio MJ, Wang S, Chernova N, Zavalij PY, Whittingham MS (2008) The hydrothermal synthesis and characterization of olivines and related compounds for electrochemical applications. Solid State Ionics 178(31–32):1676–1693. https://doi.org/10.1016/j.ssi.2007.10.015
26. Sukkabot W (2020) Effect of transition metals doping on the structural and electronic properties of $LiMnPO_4$: spin density functional investigation. Phys Scr 95(4):045811. https://doi.org/10.1088/1402-4896/ab6aff
27. Julien CM, Ait-Salah A, Mauger A, Gendron F (2006) Magnetic properties of lithium intercalation compounds. Ionics 12(1):21–32. https://doi.org/10.1007/s11581-006-0007-5
28. Kellerman DG, Chukalkin YG, Medvedeva NI, Gorshkov VS, Semenova AS (2016) Effect of vanadium doping on the magnetic properties of $LiMnPO_4$. Phys Status Solidi (b) 253(5):965–975. https://doi.org/10.1002/pssb.201552682
29. Zeng D, Cabana J, Yoon WS, Grey CP (2010) Investigation of the structural changes in $Li[Ni_yMn_yCo_{(1-2y)}]O_2$ (y = 0.05) upon electrochemical lithium deintercalation. Chem Mater 22(3):1209–1219. https://doi.org/10.1021/cm902721w
30. Rajammal K, Sivakumar D, Duraisamy N, Ramesh K, Ramesh S (2016) Effect of sintering temperature on structural properties of $LiMnPO_4$ cathode materials obtained by sol-gel method. J Sol-Gel Sci Technol 80(2):514–522. https://doi.org/10.1007/s10971-016-4111-3
31. Wen F, Shu H, Zhang Y, Wan J, Huang W, Yang X, Yu R, Liu L, Wang X (2016) Mesoporous $LiMnPO_4$/C nanoparticles as high-performance cathode material for lithium-ion batteries. Electrochim Acta 214:85–93. https://doi.org/10.1016/j.electacta.2016.08.042

32. Di Lecce D, Hu T, Hassoun J (2017) Electrochemical features of $LiMnPO_4$ olivine prepared by sol-gel pathway. J Alloy Compd 693:730–737. https://doi.org/10.1016/j.jallcom.2016.09.193
33. Xu X, Wang T, Bi Y, Liu M, Yang W, Peng Z, Wang D (2017) Improvement of electrochemical activity of $LiMnPO_4$-based cathode by surface iron enrichment. J Power Sources 341:175–182. https://doi.org/10.1016/j.jpowsour.2016.12.001
34. Fang H, Yi H, Hu C, Yang B, Yao Y, Ma W, Dai Y (2012) Effect of Zn doping on the performance of $LiMnPO_4$ cathode for lithium-ion batteries. Electrochim Acta 71:266–269. https://doi.org/10.1016/j.electacta.2012.03.160
35. Xiao J, Xu W, Choi D, Zhang JG (2010) Synthesis and characterization of lithium manganese phosphate by a precipitation method. J Electrochem Soc 157(2):A142. https://doi.org/10.1149/1.3265440
36. Han J, Yang J, Xu Z, Li H (2021) Enhancing the electrochemical performance of $LiMnPO_4$ cathode via $LiNi_{1/3}Co_{1/3}Mn_{1/3}O_2$. Ionics 27(5):1899–1907. https://doi.org/10.1007/s11581-021-03969-3
37. Pan X, Gao Z, Liu L, Xiao F, Xiao F, Xie S, Yi R (2019) Self-templating preparation and electrochemical performance of $LiMnPO_4$ hollow microspheres. J Alloy Compd 783:468–477. https://doi.org/10.1016/j.jallcom.2018.12.348
38. Wang Y, Yang Y, Yang Y, Shao H (2010) Enhanced electrochemical performance of unique morphological cathode material prepared by solvothermal method. Solid State Commun 150(1–2):81–85. https://doi.org/10.1016/j.ssc.2009.09.046
39. Zhang Z, Hu G, Cao Y, Duan J, Du K, Peng Z (2015) Enhanced electrochemical performance of nano $LiMnPO_4$ with multifunctional surface co-coating of Li_2TiO_3 and carbon. Solid State Ionics 283:115–122. https://doi.org/10.1016/j.ssi.2015.10.007
40. Ramar V, Saravanan K, Gajjela S, Hariharan S, Balaya P (2013) The effect of synthesis parameters on the lithium storage performance of $LiMnPO_4$/C. Electrochim Acta 105:496–505. https://doi.org/10.1016/j.electacta.2013.05.025